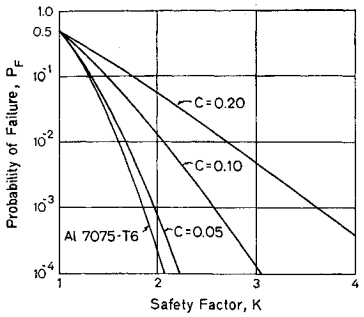

Fig. 2 Probability of failure vs safety factor for three types of scatter of fatigue strength and for 7075-T6 aluminum alloy under variable-amplitude loading.

probability of failure, we shall consider here the case of a deterministic loading for which the number of cycles $n_K(S_i)$ at each stress level is given. In practical analyses, the loading is usually specified in terms of the load spectra. If the number of stress levels is finite, the loading is said to have a discrete spectrum, in which the proportion of cycles with an amplitude S_i is $p(S_i)$. Hence, the total safe number of cycles with the amplitude S_i is

$$n_K(S_i) = L_K p(S_i) \tag{12}$$

If the number of stress levels is very large, a continuous spectrum is used in the form of a function $f(S)$, such that the number of cycles with the amplitudes between, say S_1 and S_2, is

$$n_K = L_K \int_{S_1}^{S_2} f(S)\, dS \tag{13}$$

For computational purposes, a continuous spectrum may be replaced by an equivalent discrete spectrum; for example, with

$$p(S_i) = f(S_i)\Delta S \tag{14}$$

where ΔS is the stress-amplitude interval.

In terms of $p(S_i)$ and L_K, Eqs. (10) and (11) assume the form

$$E[D] = \sum_i L_K p(S_i)/E[N(S_i)] \tag{15}$$

$$V[D] = \sum_i L_K p(S_i)\, V[N(S_i)]/E^2[N(S_i)] \tag{16}$$

Consider a material with the property

$$V[N(S_i)]/E^2[N(S_i)] = \text{const} = C \tag{17}$$

i.e., the scatter of the fatigue life is the same for every stress amplitude. In this case, from Eqs. (10) and (11) or (15) and (16),

$$E(D) = 1/K, \quad V[D] = C/K \tag{18}$$

and the probability of failure follows from Eq. (8). Figure 2 shows the relations between the probability of failure P_F and the safety factor K for three values of C.

An actual material will not, as a rule, exhibit the same scatter for every stress amplitude. Consequently, the values of $E(D)$ and $V(D)$ must be numerically evaluated from Eqs. (15) and (16), as the simple expressions (18) are no longer valid. A computation of this type has been performed for 7076-T6 aluminum alloy tested in Ref. 5, and for the load spectra given in Table III of Ref. 5, with $S_m = 0$ and $S_m =$ 10ksi. The results are given in Fig. 2. The lines corresponding to $S_m = 0$ and $S_m = 10$ ksi are very close; this may be explained by the fact that in both cases the same "gust frequency curve" has been used to establish the load spectrum.

Conclusions

The relation between the safety factor K and the probability of failure in fatigue P_F has been established with the aid of a probabilistic model of fatigue failure under variable-amplitude loading. This relation appears to be of definite significance in selecting rational values of the safety factor. Also, it may be of some help in planning the inspection, maintenance, and replacement for a fleet of aircraft. Further research is needed in the area of the probabilistic models of fatigue failure and their application to more complex, especially multiple-path, structures.

References

[1] Freudenthal, A. M., "Critical Appraisal of Safety Criteria and Their Basic Concepts," *8th Congress of International Association for Bridge and Structural Engineering*, Preliminary Publication, 1968, pp. 13–24.

[2] Freudenthal, A. M., Garrelts, J. M., and Shinozuka, M., "The Analysis of Structural Safety," Proceedings Paper 4682, *Journal of the Structural Division, ASCE*, Vol. 92, No. ST 1, Feb. 1966, pp. 267–325.

[3] Miner, M. A., "Cumulative Damage in Fatigue," *Journal of Applied Mechanics*, Vol. 12, No. 3, 1945, pp. 159–164.

[4] Parzen, E., "On Models for the Probability of Fatigue Failure of a Structure," AGARD Rept. 245, Paris, 1959.

[5] Naumann, E. C., Hardrath, H. F., and Guthrie, D. E., "Axial Load Fatigue Tests of 2024-T3 and 7075-T6 Aluminum Alloy Sheet Specimens under Constant- and Variable-Amplitude Loads," TN D-212, Dec. 1959, NASA.

An Experimental Method for Determining the Condensed Phase Heat of Reaction of Double-Base Propellants

C. E. KIRBY*
NASA Langley Research Center, Hampton, Va.
AND
N. P. SUH†
Massachusetts Institute of Technology, Cambridge, Mass.

Nomenclature

c_p = specific heat
$\bar{c}_p$ = average specific heat of gas mixture
D = mass diffusivity
E = activation energy
G = mass flux fraction
Δh_f = standard heat of formation
K = pre-exponential factor in Arrhenius expression
M = total mass flux
Q_r = condensed phase heat of reaction
R = gas constant
T = temperature
W = net rate of loss due to chemical change
x = space coordinate
Y = mass concentration fraction
λ = thermal conductivity
ρ = mass density

Introduction

AT present, no acceptable means of measuring the condensed phase heat of reaction of solid propellants exists. Some investigators have attempted to use differential scanning

Received October 19, 1970; revision received Dec. 21, 1970.

* Aerospace Engineer, Flight Vehicles and Systems Division. Member AIAA.

† Associate Professor of Mechanical Engineering.

calorimetry (DSC) for such measurements. However, Thompson and Suh[1] using high-speed motion pictures with microthermocouples and a high-response recording system and Kirby and Suh[2] using DSC and TGA techniques have shown that gas phase reactions occur very close to the surface of a deflagrating double-base propellant. Even during "flameless combustion," these gaseous reactions exist and are still close enough to the surface (less than 200 μ) to prevent their being swept away by the purge gas stream of the DSC. The DSC is, therefore, inadequate for separating condensed phase reactions from gas phase reactions if reactions occur very fast and/or very close to the burning surface of a propellant.

An indirect method for measuring the condensed phase heat of reaction using the theory of Adams[3] and the experimental technique of Suh et al.[4] will now be described.

Theory

Adams[3] has extended the theory of steady laminar flame propagation for a single chemically reacting gas to a combustion process involving several consecutive reaction steps of a solid reactant going to gaseous products. He determines the value of mass flux which allows the temperature and concentration profiles to meet the required boundary conditions imposed by the final product gases. For one-dimensional flow the mass conservation equation is

$$MdG_i/dx = W_i \tag{1}$$

the diffusion equation is given as

$$MG_i = MY_i - \rho D_i dY_i/dx \tag{2}$$

and the conservation of energy equation is

$$(d/dx)[M\Sigma G_i h_i - \lambda dT/dx] = 0 \tag{3}$$

where the component enthalpies are defined by

$$h_i = \Delta h_{f,i} + \int^T c_p dT \tag{4}$$

The assumptions are that no heat losses to the surroundings occur and that the derivatives vanish at the hot boundary as the system tends toward equilibrium. Under these assumptions, the total enthalpy approaches a constant value and the energy equation can be integrated to give

$$\lambda dT/dx = M\Sigma G_i h_i - M(\Sigma G_i h_i)_{\text{hot boundary}} \tag{5}$$

These equations are applied to a solid A undergoing an exothermic, zero-order, reaction to give a gas phase product B which then is converted to a stable product D in two stages of first and second order, respectively,

$$A \xrightarrow[\text{zero order}]{ka} B \xrightarrow[\text{first order}]{kb} C \xrightarrow[\text{second order}]{kc} D$$

It is assumed that each reaction commences only when the preceding one has been completed. Therefore in the first reaction zone $G_a + G_b = 1$, $G_c = G_d = 0$; in the second zone $G_b + G_c = 1$, $G_a = G_d = 0$; and in the third zone $G_c + G_d = 1$, $G_a = G_b = 0$. Integrating Eq. (3) and applying the mass flux fraction relations in the first reaction zone shows

$$MG_a(\Delta h_{f,a} - \Delta h_{f,b}) + M(\Delta h_{f,b} - \Delta h_{f,d}) - \lambda dT/dx = M\bar{c}_p(T_d - T) \tag{6}$$

Adams here defines a minimum surface temperature T_s' by setting the temperature gradient in the gas phase adjacent to the surface equal to zero in Eq. (6) and putting $G_a = 0$ (solid phase reaction completed) to give

$$(\Delta h_{f,b} - \Delta h_{f,d}) = \bar{c}_p(T_d - T_s') \tag{7}$$

Using this relation to eliminate T_d from Eq. (6) gives

$$MG_a(\Delta h_{f,a} - \Delta h_{f,b}) - \lambda dT/dx = M\bar{c}_p(T_s' - T) \tag{8}$$

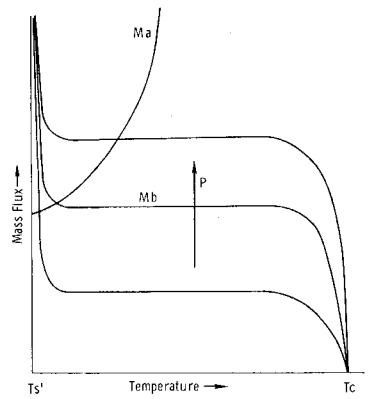

Fig. 1 Variation of mass flux and surface temperature of condensed phase with pressure.

The differential equation for G_a as a function of T is then given by

$$dG_a/dT = \lambda W_a/M^2[\bar{c}_p(T_s' - T) - G_a(\Delta h_{f,a} - \Delta h_{f,b})] \tag{9}$$

This equation is to be integrated from the cold boundary where $G_a = 1$ to the propellant surface where $T = T_s$ and $G_a = 0$. Using the relation defining the initial temperature T_0, that is,

$$\bar{c}_p(T_s' - T_0) = \Delta h_{f,a} - \Delta h_{f,b} \tag{10}$$

Eq. (9) can be written as

$$(T_s' - T)dG_a - (T_s' - T_0)G_a dG_a = (\lambda W_a/M^2\bar{c}_p)dT \tag{11}$$

The left side of this equation can also be expressed as

$$(T_s' - T_s)dG_a + (T_s - T)dG_a - (T_s' - T_0)G_a dG_a \tag{12}$$

If E_a/RT_s is large and we restrict solutions to those crossing the $G_a = 1$ line nearly horizontally, then G_a approaches unity for small values of $(T_s - T)$ so the second term is small compared with the last term. A first approximation to the solution passing through $G_a = 0$ where $T = T_s$ is given by

$$\frac{G_a^2(T_s' - T_0)}{2} - (T_s' - T_s)G_a = \frac{1}{M^2\bar{c}_p}\int_T^{Ts} \lambda W_a dT \tag{13}$$

and an approximate value of the mass flux can be found by letting $G_a = 1$ in this equation. We can assume $W_a = \rho_a K_a \exp(-E_a/RT)$ and that the term on the right-hand side can be written as

$$\frac{\lambda_a \rho_a K_a}{M^2\bar{c}_p}\int_T^{Ts} \exp(-E_a RT)dT \tag{14}$$

This integral is not sensitive to the value of the lower limit T and a first approximation for the mass flux is

$$M^2 = [2\lambda_a\rho_a K_a/\bar{c}_p(2T_s - T_s' - T_0)](RTs^2/E_a) \times \exp(-E_a/RT_s) \tag{15}$$

Adams then treats the next stage of the flame by a similar procedure and provides a graphical solution for the system as reproduced in Fig. 1. The mass flux for the coupled system, and the value of T_s, is determined by the intersection of two curves. The condensed phase curve Ma is independent of pressure but the curves for the first-order gas reaction Mb are shifted vertically upward as the pressure increases. At low pressures, notice that the intersections occur on the nearly vertical portion of the Mb curve where T_s approaches T_s', the minimum surface temperature with no heat feedback from the gas phase. The burning rate is then effectively that of the adiabatic condensed phase reaction.

At the time Adams provided this analysis he did not have an experimental value of T_s' to use, as indicated by his solution of a sample problem on p. 143 of Ref. 3, and the following direct quotation: "The heat release of the solid phase re-

action and therefore the adiabatic surface temperature T_s' are not known but the calculation is relatively insensitive to the possible variation in these parameters. We shall assume $(T_s' - T_0)$ equal to 250°C corresponding to a heat of reaction in the solid phase of approximately 90 cal/g."

Experiment

We now have an experimental method for measuring the value T_s' to use in Adams' theory to calculate the condensed phase heat of reaction.

Briefly, the method suggested by Suh et al.[4] consists of raising the initial temperature of the propellant to various desired temperatures uniformly by passing hot air around it and measuring the burning rates. Figure 4 of Ref. 4 shows the experimental results for burning rate as a function of initial temperature. The asymptotic temperature at which the burning rate approaches infinity is found to be 145°C (290°F).

This is the minimum surface temperature at the solid surface with no heat feedback from the gas phase. The experimental arrangement indicates that if a piece of propellant is heated to 145°C, it is just about to ignite by itself and the slightest amount of energy which is added to it externally results in sudden ignition and rapid deflagration at a rate approaching infinity. This is therefore the temperature at which no heat feedback from the flame is necessary and it does burn at a rate approaching infinity just as Eq. (15) predicts that it should.

Discussion

It is important to remember that the temperature T_s' does not actually exist at the burning surface during the experimental procedure described herein and it may actually never exist at the surface of a steady-state burning propellant. We are not determining T_s' from a direct measurement of the surface temperature itself (which may be impossible with present technology) but asymptotically with an indirect measurement from the other end of the flame front which is much more reliable experimentally, and which logically does meet the requirement of no heat feedback from the gas phase.

The possibility of condensed phase reactions occurring during the experiments while the propellant sample is being heated to a desired initial temperature has been suggested. However, Ref. 2 indicates that at a heating rate of 20°C per minute, which is approximately the rate at which the propellant samples were usually heated, significant heat generation does not occur until temperatures are above 165°C.

Conclusions

The method presented in this paper provides a simple technique for isolating the condensed phase contribution to the over-all heat of reaction of a deflagrating double-base propellant. With M-2 type propellant for which T_s' is 145°C, $\bar{c}_p = 0.37$, and assuming an initial temperature of $T_0 = 25$°C we obtain

$$Q_r = 0.37(145 - 25) = 45 \text{ cal/g}$$

References

[1] Thompson, C. L. and Suh, N. P., "Gas Phase Reactions Near the Solid-Gas Interface of a Deflagrating Double-Base Solid Propellant," *AIAA Journal*, Vol. 9, No. 1, Jan. 1971, pp. 154–159.

[2] Kirby, C. E. and Suh, N. P., "Reactions Near The Burning Surface of Double-Base Propellants," *AIAA Journal*, Vol. 9, No. 2, Feb. 1971, pp. 317–320.

[3] Adams, G. K., "The Chemistry of Solid Propellant Combustion: Nitrate Ester of Double-Base Systems," *Proceedings of the 4th Symposium on Naval Structural Mechanics*, Purdue Univ., Lafayette, Ind., April 1965. pp. 117–147.

[4] Suh, N. P. et al., "Ignition and Surface Temperature of Double-Base Propellants at Low Pressure I—Thermocouple Measurements," *AIAA Journal*, Vol. 8, No. 7, July 1970, pp. 1314–1321.

Laminar Incompressible Flow Past a Circulation-Controlled Circular Lifting Rotor

ALLEN PLOTKIN*

University of Maryland, College Park, Md.

Introduction

IN the flow past a lifting body, the lift predicted from potential flow considerations is usually not realized due to boundary-layer separation. One way to alleviate this problem is to introduce a tangential jet to postpone the onset of separation.

To study the problem of flow past a body with circulation control, the problem of a jet on a curved surface in the presence of an external stream must be considered. Numerical solutions for the laminar, two-dimensional, high Reynolds number case with no external pressure gradient have been obtained by Pai and Hsieh[1] and Kleinstein[2] for the freejet and straight wall jet, respectively. Schetz and Jannone[3] have considered the effect of an upstream boundary layer for the straight wall case.

Methods of solution have been presented for treating the turbulent flow past circulation-controlled rotors. Among these investigations are the circular cylinder of Dunham[4] and the elliptic cylinder of Kind.[5] The turbulent problem involves the introduction of much empirical information. It is for this reason that the laminar case is studied in the hope that important trends can be predicted that compare favorably with experimental observations.

Laminar Incompressible Jet on a Circular Cylinder

The flow configuration is shown in Fig. 1. θ is the angle measured from the forward stagnation point and the blowing slot is situated at $\theta = 90°$. The speeds of the uniform stream and the jet are U and U_j, respectively. The cylinder radius is R and the slot height is h.

The equations to be solved are the first-order boundary-layer equations of Prandtl for two-dimensional, laminar, incompressible flow. The outer inviscid flow is the potential flow solution for the cylinder without the jet. The equations are solved numerically using the implicit finite-difference scheme of Blottner and Flügge-Lotz.[6]

The jet strength can be varied by changing either U_j or h. Experimental results are usually correlated using the momentum coefficient $C_\mu = hU_j^2/2RU^2$ as the jet parameter. The suitability of this parameter will be investigated.

For now, the boundary layer upstream of the slot is not taken into account. Its effect will be studied later. The

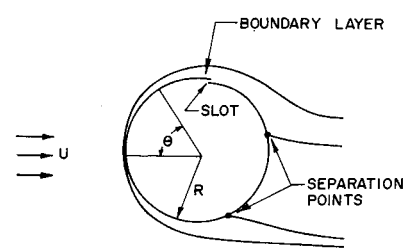

Fig. 1 Schematic representation of the flow.

Received November 20, 1970. The computer time for this project was supported in part by NASA Grant NsG-398 to the Computer Science Center of the University of Maryland. The research was supported in part by NASA Grant NGR 21-002-266 with Ames Research Center.

* Assistant Professor of Aerospace Engineering. Member AIAA.